Applied Surface Science 609 (2023) 155253

Contents lists available at ScienceDirect

Applied Surface Science

journal homepage: www.elsevier.com/locate/apsusc

Full Length Article

Features of the surface layer structure of the magnetosensitive materials functionalized by silica with thiourea groups and their applying for selective Cu(II) and Au(III) ions removal

Inna V. Melnyk [a,b,*], Miroslava Vaclavikova [a], Lucia Ivanicova [a], Maria Kanuchova [c], Gulaim A. Seisenbaeva [d], Vadim G. Kessler [d]

[a] Institute of Geotechnics, Slovak Academy of Sciences, 45 Watsonova, Košice 04001, Slovak Republic
[b] Chuiko Institute of Surface Chemistry, National Academy of Sciences of Ukraine, 17 Generala Naumova, Kyiv 03164, Ukraine
[c] Technical University of Košice, 9 Letna, Košice 04200, Slovak Republic
[d] Swedish University of Agricultural Sciences, Box 7015, 5 Almas allé, Ultuna, Uppsala 75007, Sweden

ARTICLE INFO

Keywords:
Magnetite particles
Sol-gel technique
Thiourea groups
Cu(II) adsorption
Au(III) adsorption
Selective adsorption

ABSTRACT

One-step sol–gel synthesis for covering magnetic particles with polysiloxane layers with $\equiv Si(CH_2)_3NHC(S)NHC_2H_5$ groups has been proposed. Unique properties of this functional group, containing sulfur and nitrogen, and the developed approach open wide (and novel) opportunities for the controlled surface design. A number of factors affecting the characteristics of such materials and their sorption properties towards heavy metal ions were analyzed. Results of scanning and transmission electron microscopy studies, Fourier-transform infrared spectroscopy, nitrogen adsorption–desorption measurements, elemental analysis, thermogravimetric analysis, and X-ray powder diffraction analysis indicated that, depending on the ratio of core/shell components, the resulting spherical moieties with size of 35.1–43.1 nm, can form agglomerates of larger sizes. Packing of these aggregates offers porosity to such materials, having a dense or loose polysiloxane shell, with thiourea groups load of 0.67–1.05 mmol/g. The synthesized materials proved to be effective in extraction of Cu(II), Pb(II), Cd(II), Hg(II), Ag(I), Au(III), Zn(II) ions from aqueous solutions, as well as in selectively adsorption of Au(III) ions at pH = 3 and Cu(II) ions at pH = 5.5. X-ray photoelectron spectroscopy demonstrated different types of interactions between metal ions and the thiourea groups, depending on pH.

1. Introduction

Exceptional magnetic properties and nano size of magnetite offer its versatile use. Over the past fifteen years, magnetic nanoparticles have been widely implemented in medicine [1], catalysis [2], biotechnology [3], and also in sorption [4]. Magnetite is a fairly stable compound, exhibits superparamagnetic properties, and therefore, when an external magnetic field is applied, it can easily be removed from the solution. However, when heated to 150 °C, it turns into iron(III) oxides, can be oxidized in the process of aeration, and is sensitive to changes in the pH in solution [5]. Magnetite nanoparticles are capable also of aggregation and sedimentation, urging for further research in the field of functionalization of magnetic particles, their uniform coating with oxides, polymers, etc., in order to preserve magnetic properties and expand the areas of applications. Therefore, magnetic composite materials can be applied to solve more specific tasks [6]. Functionalization of the magnetite with polysiloxane layers is important for adsorption of metal ions from aggressive environments, especially because the polysiloxane shells are inorganic polymers (usually obtained in one step) showing good resistance to highly acidic environments [7], and are not swelling in organic solvents. In addition, it is possible to provide such materials with specific properties during the one-step synthesis by introducing different functional groups [8].

Sulfur-functionalized silica adsorbents attract much attention due to their ability to adsorb ions of precious [9] and heavy metals [10]. Selectivity of such adsorbents is much higher than of the oxygen-containing analogs [11]. Moreover, sulfur-functionalized silica can be used in chromatography for separation of optical isomers [12] and for the adsorption of enzymes [13]. They are also convenient for immobilization of biologically active compounds [14]. Indirectly, the

* Corresponding author at: Institute of Geotechnics, Slovak Academy of Sciences, 45 Watsonova, Košice 04001, Slovak Republic.
E-mail address: in.melnyk@gmail.com (I.V. Melnyk).

https://doi.org/10.1016/j.apsusc.2022.155253
Received 26 July 2022; Received in revised form 12 September 2022; Accepted 7 October 2022
Available online 19 October 2022

irreversible adsorption of stable metal complexes with fixed sulfur-containing ligands on porous supports presents an opportunity for their application in heterogeneous catalytic systems [15]. N-containing silica materials proved themselves as adsorbents of inorganic and organic pollutants, antibacterial agents, and as carriers of biocatalysts [16].

Three main approaches to magnetic nanoparticles covered with silica layer are described in the literature. The first method, known as the sol–gel process, is based on the use of silicon alkoxides [17] and silicates [18] as sources of the polysiloxane layer. According to this technique, the silica phase is formed on colloidal magnetic nanoparticles in an alcohol-water medium in an alkaline environment. The second approach is based on the formation of magnetic particles inside the pores of previously synthesized silica using metal compounds (salts or alkoxides) as a source of the magnetic phase [19]. According to the third technique, non-ionic surfactants were used for the formation of the reverse microemulsion to separate or suspend magnetic nanoparticles, while a layer of silica was formed around them by hydrolysis and condensation of tetraethyl orthosilicate (TEOS) [20].

Among the specified methods for the synthesis of silica-functionalized magnetic nanoparticles, sol–gel synthesis is used most often due to relatively mild reaction conditions, low costs, and the absence of extraneous substances (surfactants), which must be removed at the next stages of synthesis. Organosilanes can be considered as ideal precursors for the synthesis of functionalized silicas because their chemical composition is widely variable. Organosilanes that contain both S and N functions are therefore very well suitable for the synthesis of selective adsorbents with both chemical functions present as active surface anchors [21]. Selectivity and capacity of such adsorbents towards metal ions will largely depend on the number and position of the functions [22], which is also observed for other materials during selective adsorption of the adsorbates of different natures [23,24]. Thus thiocarbamide groups can form stable complexes with metal ions and, for example, protect the surface of copper by combining allylthiourea and some silanes forming a hybrid sol–gel coating [25,26], and could sorb metal ions from aqueous solutions [27,28]. Therefore, the one-pot synthesis of such adsorbents is highly appealing. Such synthesis can be made by sol–gel technique of polymerizing and gelling of carefully selected organosilanes. In this way, one should be able to obtain both the high surface concentration of active groups and the required porous structure. Thus, such approach opens wide (and new) opportunities for the controlled surface design.

Thus, in this article, we decided to develop a method for the synthesis of magnetosensitive nanoparticles containing thiourea groups of the composition $Fe_3O_4/SiO_2/{\equiv}Si(CH_2)_3NHC(S)NHC_2H_5$, and to identify the factors affecting the characteristics of such materials and their sorption properties towards heavy metal ions. The use of magnetic particles with a coating of functionalized silica makes possible, first, to selectively adsorb target components from the solution, and second, to separate nanocomposites with bound metals from the solution with the help of a magnet, which is impossible to realize if using sorbents without a magnetic core. The structure of such composites and the composition of their surface layer were established, sorption properties, competitive adsorption, and concentration of copper and gold ions from natural waters were also studied. It is shown that magnetic composites obtained in a simple way can be highly effective selective adsorbents for copper and gold ions.

2. Materials and methods

2.1. Reagents

Following substances were used as synthesis precursors: tetraethoxysilane, $Si(OC_2H_5)_4$ (TEOS, 98%, Aldrich); 3-aminopropyltriethoxysilane, $(C_2H_5O)_3Si(CH_2)_3NH_2$ (APTES, 99%, Aldrich); ethylisothiocyanate, C_2H_5NCS (EtNCS, 97%, Aldrich); ethanol (EtOH, 99.5%, Solveco); iron(II) chloride, $FeCl_2$ (98%, Aldrich); iron(III) chloride, $FeCl_3$ (98%, Merck); ammonium fluoride, NH_4F (98%, Fluka); ammonia, NH_4OH (25%, Merck).

Following substances were used to study sorption: mercury(II) nitrate monohydrate, $Hg(NO_3)_2{\cdot}H_2O$ (anal. grade, Macrochem, Ukraine); silver(I) nitrate, $AgNO_3$ (anal. grade, Macrochem, Ukraine); hydrogen tetrachloroaurate hydrate, $H[AuCl_4]{\cdot}H_2O$ (99.999%, trace metals basis, Acros Organics); cadmium(II) nitrate tetrahydrate, $Cd(NO_3)_2{\cdot}4H_2O$ (99%, ITES s.r.o., Slovakia); zinc(II) nitrate hexahydrate, $Zn(NO_3)_2{\cdot}6H_2O$ (pure p.a., POCH s.a., Poland); copper(II) nitrate trihydrate, $Cu(NO_3)_2{\cdot}3H_2O$ (98%, ITES s.r.o. Vranov, Slovakia); lead(II) nitrate, $Pb(NO_3)_2$ (pure p.a., Lachema a.s., Czech Republic); cobalt(II) sulfate heptahydrate, $CoSO_4{\cdot}7H_2O$ (99%, Lachema a.s., Czech Republic); nickel(II) sulfate hexahydrate, $NiSO_4{\cdot}6H_2O$ (pure, Lachema a.s., Czech Republic); sodium nitrate, $NaNO_3$ (anal. grade, ITES s.r.o. Vranov, Slovakia); ammonium chloride NH_4Cl and sodium chloride NaCl (chemically pure, Macrochem, Ukraine); nitric acid, HNO_3 (fixanal concentrates, Reachem, Ukraine); ethylenediaminetetraacetic acid, $C_{10}H_{16}N_2O_8$ (EDTA) (fixanal concentrates, Reachem, Ukraine); magnesium sulfate, $MgSO_4{\cdot}7H_2O$ (fixanal concentrates, Reachem, Ukraine); eriochrome black T (anal. grade, Reanal, Ukraine); thiourea, NH_2CSNH_2 (99%, Lachema a.s., Czech Republic).

2.2. Synthetic approaches

Synthesis of trifunctional silane $(C_2H_5O)_3Si(CH_2)_3NHC(S)NHC_2H_5$ (ETUS) was carried out according to reference [29]. Thus, the solution of 4.4 mL (0.05 mol) of ethylisothiocyanate in 20 mL of C_2H_5OH was added under vigorous stirring to 11.7 mL (0.05 mol) of APTES dissolved in 30 mL of C_2H_5OH (99.5%) in a Schlenk flask (nitrogen atmosphere). The solution was refluxed at 60 °C for 1 h and, after cooling to room temperature, the solvent was removed in vacuum. The resulting solid white substance had the yield 15.66 g.

Magnetite was prepared by co-precipitation of iron(II) and iron(III) chlorides with ammonia, in a nitrogen atmosphere [30]. Iron(II) chloride (5.489 g, 0.043 mol) and iron(III) chloride (14.169 g, 0.087 mol) were dissolved in 450 mL of distilled water at 80 °C under nitrogen flow. Then, 50 mL of ammonia solution was added to the reaction mixture. The black precipitate was produced and kept under 80 °C with mechanical stirring during 30 min. After this time, the heating was stopped, suspension was cooled to room temperature. The magnetite nanoparticles were separated from the solution by decantation using a permanent neodymium magnet. In order to remove the residual solvents, the magnetite particles were cleaned by repeated cycles of washing with water and ethanol. After washing the magnetite, ethyl alcohol was added and the formed suspension was stored for further functionalization.

*Synthesis of magnetite-silica-thiourea (***MSTU***) composites.*

Sample **MSTU 1**. First, 3.6 mL (0.016 mol) of TEOS were hydrolyzed in 2.0 mL of 0.0024 M hydrochloric acid and 14 mL of ethanol at 80 °C for 20 min. Separately, 0.4101 g (0.0013 mol) of ETUS were dissolved in 5 mL of ethanol and 1 mL of 1% NH_4F as catalyst under constant stirring for 4 h. Then, the magnetite suspension was prepared: 100 mg (0.0004 mol) of Fe_3O_4 in 20 mL of EtOH (99.5%) and 30 mL of H_2O (treated by ultrasound for 10 min). Solutions of TEOS (by drops) and pre-hydrolyzed ETUS were then added to magnetite suspension, under continuous stirring.

Sample **MSTU 2**. The recipe of preparation was similar to sample **MSTU 1**, but changing the ratio between the reagents to Fe_3O_4/TEOS/ETUS = 0.0004/0.013/0.0013.

Sample **MSTU 3**. The recipe of preparation was similar to sample **MSTU 1** with the ratio between the reagents Fe_3O_4/TEOS/ETUS = 0.0004/0.008/0.0013.

The formed heterogeneous systems were stirred for 4 h. The dark brown sediments were separated by magnet, rinsed three times with water (50 mL) and twice with ethanol (50 mL). The materials were dried

at ~ 100 °C in an oven for 24 h. Contrary to the other samples, **MSTU 1** appeared to be a viscous-like suspension after the stirring was stopped, so it was centrifuged. The precipitates were treated with ultrasound before drying.

2.3. Adsorption experiments

Individual metal ions adsorption from water solutions was carried out in a static mode (m = 0.01 ± 0.0005 g, V = 10 mL, t = 25 °C, τ = 18 h. The initial solution pH values were: pH ~ 2.0 for Hg^{2+}, Ag^{+}, $[AuCl_4]^{-}$; pH ~ 5.0 for Pb^{2+} and Cu^{2+}; pH ~ 6–6.5 for Cd^{2+}, Zn^{2+}, Co^{2+}, and Ni^{2+}). The ionic strength of the solution was 0.1, created by adding 1 N solution of $NaNO_3$. After the sorption, the precipitates were washed three times by 5 cm^3 of distilled water, and the content of metals was determined in the filtrate. All metal ions concentrations, except Hg(II), both in the initial solutions and in the filtrates were determined with Varian AA 240 FS Fast Sequential Atomic Absorption spectrometer. Hg^{2+} content was determined by back complexation titration of the excessive EDTA with 0.05 M solution of $MgSO_4$.

The sorption capacity (A, mmol/g) and the distribution coefficients (K_d, mL/g) were calculated using the formulas: $A = \frac{(C-C_{eq})\times V}{m}$ and $K_d = \frac{(C-C_{eq})\times V}{C_{eq}\times m}$, where C and C_{eq} are the initial and equilibrium concentrations of metal ions in the aqueous phase, respectively, mol/L; V is the volume of solution, mL; m is adsorbent mass, g.

Adsorption kinetics was described using the pseudo-first order $\ln(A_{eq}-A_t) = \ln A_{eq} - k_1 t$ and the pseudo-second order $t/A_t = 1/k_2 A_{eq}^2 + t/A_{eq}$ rate laws, where A_{eq} and A_t are the adsorption capacities (amounts of metal ions adsorbed on the adsorbent) at equilibrium and at time t; k_1 and k_2 are the pseudo-first and pseudo-second order rate constants, $h = k_2 A_{eq}^2$ is an initial sorption rate assuming the pseudo-second kinetic order model.

Langmuir $C_{eq}/A_{eq} = 1/K_L A_{max} + C_{eq}/A_{max}$ and Freundlich $lnA_{eq} = \ln K_F + (1/n) lnC_{eq}$ isotherm models were employed to correlate the adsorption data. Here C_{eq} was equilibrium concentration of adsorbate in the solution, mg/L; A_{eq} - adsorption capacity at equilibrium, mg/g; K_L - Langmuir adsorption equilibrium constant; A_{max} - maximal adsorption capacity for complete monolayer covering of the surface; K_F - Freundlich constant; n in the Freundlich equation is an empirical parameter connected to the intensity of adsorption and heterogeneity of the adsorbent.

Selective adsorption from mixtures of ions (Au^{3+}, Cu^{2+}, Pb^{2+}, Cd^{2+}, Zn^{2+}, Ni^{2+}, Co^{2+}) or (Cu^{2+}, Pb^{2+}, Cd^{2+}, Zn^{2+}, Ni^{2+}, Co^{2+}) was carried out in a dynamic mode (m = 0.025 ± 0.0005 g, V = 25 mL, initial solution pH ~ 3.0 or pH ~ 5.5, ionic strength ~ 0.1). The capped polyethylene vials with suspensions were placed inside a constant orbital shaker at room temperature. The samples were collected in 24 h, filtered through the paper filters, and the metal ions concentrations were quantified by Varian AA 240 FS Fast Sequential AAS.

Concentrating of Au(III) was carried out in a dynamic mode with a sample concentration of 1 g/L, stirring time of 2 h, from a mixture of ions containing 12.66 mg/L of Au(III), 16.7 mg/L of Cu(II), 18.5 mg/L of Pb (II), 20.0 mg/L of Cd(II), 22.3 mg/L of Zn(II), 16.0 mg/L of Ni(II), and 24.2 mg/L of Co(II). The sorbent was removed from the suspension with a magnet after agitation with the solution for 2 h each cycle, and it was filled with a new initial solution without washing and regeneration. This was repeated 24 times (24 cycles of adsorption).

Regeneration of Au- and Cu-loaded materials was also performed in the dynamic mode by 4% thiourea solution in 120 min with a sample concentration 1 g/L. Thiourea solution was prepared using a solvent mixture of 1 M HNO_3 and ethanol 4/1 (v/v). After that, the thiourea was mineralized and the acid solution of the metal ions was analysed. For desorption of Hg(II) ions was used a solution of EDTA (0.025 M) and 0.1 M nitric acid in a ratio of 3/7 (v/v) with a sample dosage of 1 g/L was used for 24 h. The concentration of desorbed Hg(II) was determined by a complexometric titration with EDTA.

Concentrating of Au(III) and Cu(II) from river water (Hýľov region, Slovakia, 48.726, 21.069) was carried out in a dynamic mode at temperature ~ 5 °C for 6 days. The examined sample **MTSU 2** (3 g) was placed in a plastic tube with a paper filter at the end. Water from the river was supplied with a flow rate of 50 mL/min self-flowing (Fig. SM1). The adsorbed gold and copper ions were transferred to the solution by dissolving of 1 g of the sample in 25 mL of concentrated nitric acid and concentrated hydrochloric acid 1/3 (v/v). The adsorption efficiency of metal ions from river water concentrate was also checked. The water concentrate was prepared from 5 L of river water by evaporation to 200 mL and by filtration through a paper filter (Whatman). The metal ions concentrations were quantified by inductively coupled plasma-mass spectrometry (ICP-MS) (Agilent Technologies 7700 Series).

2.4. Characterization

Scanning electron microscopy (SEM) images were obtained using analytical scanning electron microscope JEOL JSM-6060 LA. Transmission electron microscopy (TEM) images were collected on JEOL JEM 2010-Fx electron microscope at an electron beam acceleration voltage of 200 kV. The contents of C, N, and S were evaluated by elementary analyzer Vario MACRO cube (Elementar analysensysteme GmbH, Germany) using a thermal conductivity detector. The estimation of Si, Fe, and S amounts was carried out by a SEM-EDS (Scanning Electron Microscopy with Energy Dispersive Spectroscopy) technique using a Hitachi TM-1000-μ-DeX tabletop scanning electron microscope. ^{1}H NMR spectrum of trifunctional silane was recorded on a Bruker AC-300 spectrometer. DRIFT (Diffuse Reflectance Infrared Fourier Transform) spectra were recorded on a spectrometer Thermo Nicolet Nexus FTIR (Fourier-transform infrared) using diffuse reflectance 'SMART Collector'; the samples were mixed with KBr at 1:30 ratio. The initial silane (ETUS) was analysed by placing a drop between NaCl glass plates and then measuring in transmittance mode. Thermogravimetric analysis (TGA) was carried out in a Perkin-Elmer Pyris-1 TGA instrument connected with gas analysis unit operated with a Perkin-Elmer Spectrum 100 FTIR instrument. XRD (X-ray diffraction) data were obtained using a Bruker SMART APEX-II diffractometer equipped with MoKα radiation (λ = 0.71073 Å). N_2 adsorption–desorption isotherms were measured with a Kelvin-1042 instrument (Costech Microanalytical, Estonia) at –196 °C; the samples were pre-degassed at 110 °C for 3 h; the specific surface areas were calculated by the BET method. Photon cross-correlation spectroscopy (PCCS) was used to analyse and plot the distributions of particle sizes, which was performed using a Nanophox particle size analyser (Sympatec, Germany); aqueous suspensions of samples dispersed in an ultrasonic bath were used for PCCS measurement. Electrokinetic potentials (ξ-potential) of dilute suspensions of sorbents (5 mg of a sample was suspended in 5 mL of 0.001 M $NaNO_3$) in a wide pH range were studied using the analyser ZetaSizer Nano ZS (Malvern Instruments, UK). The X-ray photoelectron spectroscopy (XPS) was performed on an XPS instrument SPECS (SPECS GmbH, Germany, Berlin) equipped with PHOIBOS 100 SCD and non-monochromatic X-ray source. The survey surface spectrum of samples was scanned at 70 eV transition energy and core spectra at 30 eV and room temperature. All the spectra were obtained at a basic pressure of 1×10^{-8} mbar with Mg Kα excitation at 10 kV (200 W). The data analysis was carried out with SpecsLab2 CasaXPS software (Casa Software ltd.). The spectrometer was calibrated against silver (Ag 3d).

3. Results and discussion

3.1. Structure and surface chemistry of magnetic composites

In order to carry out a one-step synthesis, the silane with a thiourea group was synthesized first. Some authors conduct surface syntheses to obtain materials with thiourea groups [28,31], but this does not increase the sorption capacity and adds to the problems of accurate identification of reaction products. Thus, the well-known reaction of primary amines

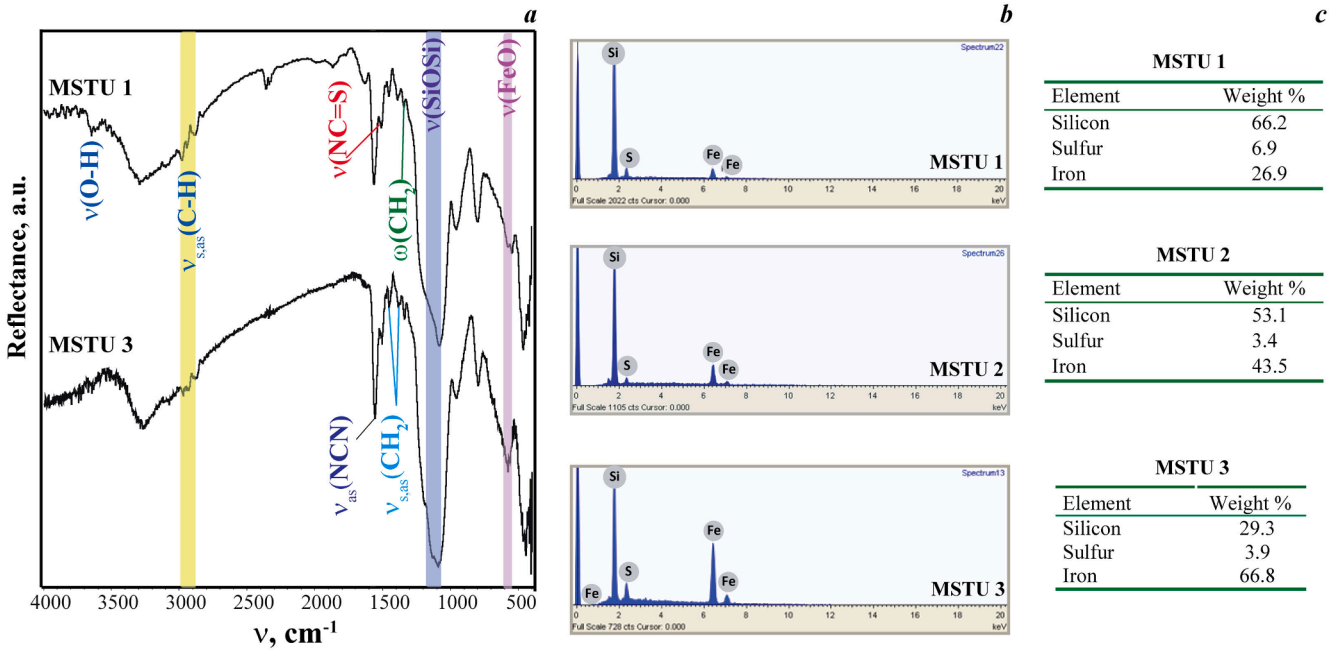

MSTU 1

Element	Weight %
Silicon	66.2
Sulfur	6.9
Iron	26.9

MSTU 2

Element	Weight %
Silicon	53.1
Sulfur	3.4
Iron	43.5

MSTU 3

Element	Weight %
Silicon	29.3
Sulfur	3.9
Iron	66.8

Fig. 1. DRIFT spectra (*a*), SEM-energy-dispersive spectra (*b*), and SEM-energy-dispersive analysis data (*c*) for magnetic materials with thiourea groups.

(APTES in our case) with organic isothiocyanates (C_2H_5NCS) was used to obtain a pure solid product soluble in ethanol, that was a silane with thiourea group $(C_2H_5O)_3Si(CH_2)_3$–NH–C(=S)–NH–C_2H_5, and its composition was confirmed by ^{1}H NMR and IR spectroscopies. ^{1}H NMR ($CDCl_3$, δ/ppm): 0.63 (t, SiCH_2), 1.20 (s, CH_3CH_2O, CH_3CH_2N), 1.69 (t, SiCH$_2$CH_2), 3.44 (s, Si(CH$_2$)$_2$CH_2N, CH$_3$CH_2N), 3.78 (qua, CH_2O), 5.76 (m, NHC$_2$H$_5$), 5.97 (m, (CH$_2$)$_3$NH) (Fig. SM2). IR, cm^{-1}: 3342w (νNH), 2975, 2932, 2881 (νCH), 1556sh (ν_{as} NCN), 1453 ($\delta_{as}CH_3$), 1385 (δ_sCH_3), 1333 (ωCH$_2$), 1269 m (ν_s NCN + νNH), 1161st (νC = S), 1092, 1044 (νSiO), 799 (νC-S) (Fig. SM3). In the view that the obtained silane had high hydrolytic stability, it could be used for the syntheses in air [21].

One-step synthesis of the magnetosensitive materials functionalized by silica with thiourea groups has its own features. Although ETUS silane is derived from APTES and also contains sulfur, the syntheses developed for materials with amino [32] and mercapto [13] groups in aqueous solution could not be performed due to salting out of ETUS, whereas the magnetite could not be functionalized in ethanol only. Thereby, the optimal water/ethanol ratio to conduct the synthesis was determined. The choice of catalyst was made on the basis of experimental studies and previous experience [13,32–33]. Using only hydrochloric acid as a catalyst, magnetic functional material was not produced

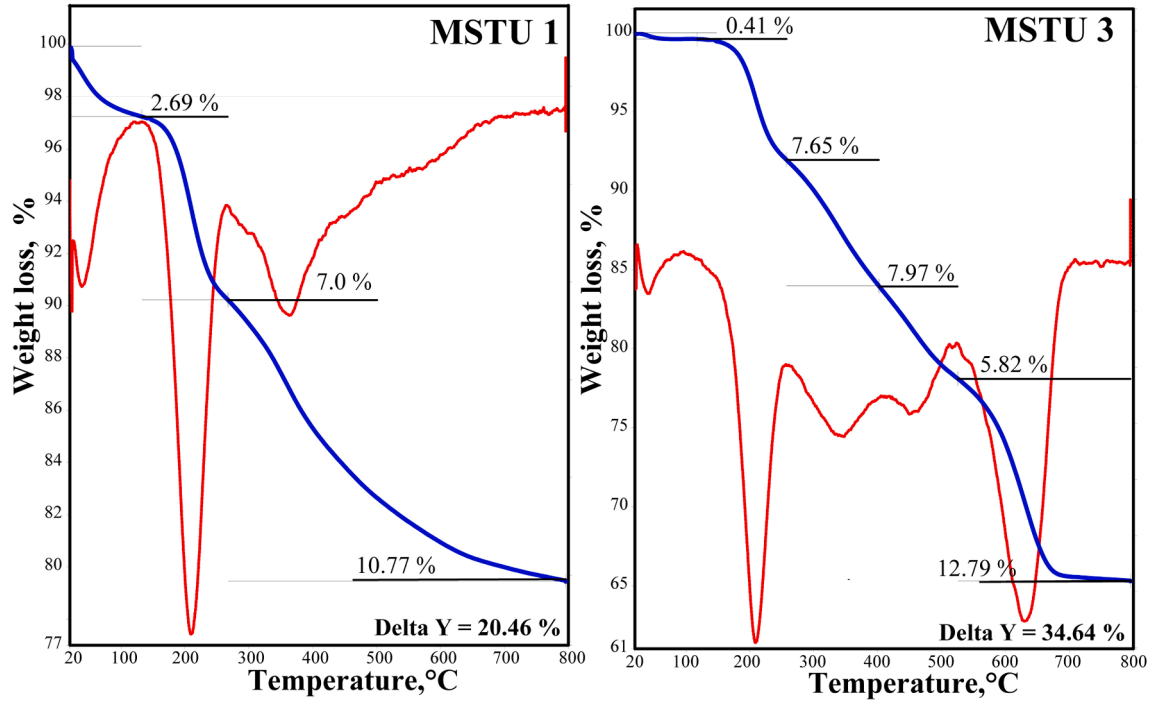

Fig. 2. Thermal analysis of the **MSTU 1** and **MSTU 3** samples.

Table 1
The content of functional groups of magnetic particles functionalized by thiourea groups.

Sample	Elemental analysis data, mass%			Content of thiourea groups, mmol/g				pI	$d_{part.}$, nm (XRD)	$d_{part.}$, nm (PCCS)	$S_{sp.}$, m^2/g
	C	N	S	N el.an.	S el.an.	TGA	SEM-EDS				
MSTU 1	8.5	2.8	3.0	1.00	0.94	1.20	2.15	5.8	43.1	253	333
MSTU 2	5.8	1.7	2.0	0.61	0.63	0.80	1.06	5.5	41.2	253	486
MSTU 3	5.2	1.9	2.1	0.68	0.66	not determined	1.22	3.1	35.1	110	94

according to the SEM-EDS data and the product yield. HCl was used also at one of the stages of synthesis for prehydrolysis of TEOS [13]. The catalyst for ETUS was chosen to be ammonium fluoride, previously used to obtain xerogels [34] and bridged xerogels [35] with thiourea groups, in such a quantity that the gelation occurred within 4 h. So, all these parameters were determined and utilized for the synthetic procedure.

In the preparation of xerogels with thiourea groups, the ratio between structure agent and ETUS affected the porosity, the concentration of functional groups, and the sorption capacity [34]. It was shown that with a decrease in ETUS in the reaction mixture, the values of specific surface area increased and the number of functional groups decreased, while the sorption capacity to mercury increased. That is, it is necessary to find such a balance in the ratio, when the developed surface has the largest number of functional groups available for interaction. In this regard, for the composites described in the current paper, the magnetite/TEOS ratio was 1/20 and more because such amount of TEOS can protect magnetite nanoparticles in acid environment [7], while the TEOS/ETUS ratio was varied.

Functionalization of magnetic particles was attested by the infrared spectra, which are presented in Fig. 1a (only for two samples because all spectra are similar). The absorption band at ~ 600 cm^{-1} was assigned to ν(Fe-O) stretching vibrations of magnetite [5]. All samples had the most intense absorption band around 1050–1200 cm^{-1} from ν_{as}(Si-O-Si) vibrations, indicating the formation of polysiloxane network in the synthesized samples. There is a group of low-intensity bands in the frequency range of 1300–1450 cm^{-1} related to the bending vibrations of the methyl and methylene groups from the propyl and ethyl fragments of the precursor. Symmetric and asymmetric stretching vibrations of C—H from methylene groups were recorded in the IR spectra as low-intensity absorption bands in the region of 2800–3000 cm^{-1}. The assignment of absorption bands in the range of 1560–1610 cm^{-1} had significate value; the bands in this region could be assigned as ν(NC = S) vibrations at 1508 cm^{-1} and ν_{as}(NCN) at 1558 cm^{-1} [31]. So, based on IR spectroscopy data, the composites consisted of magnetite/silica/thiourea groups, $Fe_3O_4/SiO_2/{\equiv}Si(CH_2)_3NHC(S)NHC_2H_5$.

The presence of Fe, Si, and S in the composites was also confirmed by SEM-EDS analysis (Fig. 1b,c). Moreover, the expected Si/Fe ratio remains unchanged during the synthesis, which indicated the formation of thicker polysiloxane shells in the range of samples **MSTU 1** > **MSTU 2** > **MSTU 3**. Regarding the thiourea moieties (by way of comprised sulfur), the highest content of them was observed in the **MSTU 1** sample, presumably because there was a possibility of ETUS co-condensation with more TEOS. The SEM-EDS spectrum of the **MSTU 3** sample contained three peaks assigned to Fe, at about 0.9, 6.3, and 7.0 keV, which corresponded to the binding energies of Fe in magnetite [35] and confirmed the presence of free locations of the later.

There were detected several transitions/effects (Fig. 2) with thermal analysis for these samples. Thus, there was observed a weight loss in the range of temperatures until 100 °C, which was connected with the removal of the residues of adsorbed water and ethanol. DTG curve recorded a significant weight loss process in the range of 200–300 °C due to the oxidation of sulfur-containing fragments. Finally, the weight loss around 400 °C was connected with the complete burning out of the organic component. For the sample **MSTU 3** we could see that its weight continued to decrease with increasing temperature, which could be due to the oxidation of magnetite [36] and indicated incomplete polysiloxane coating layer. These data correlated with the SEM-EDS analysis for the sample **MSTU 3** above.

Table 1 shows the content of the introduced functional groups calculated from the data of different methods. The amount of thiourea groups was estimated using the elemental analysis, DTA, and SEM-EDS. It could be seen that elemental analysis and DTA data correlated within

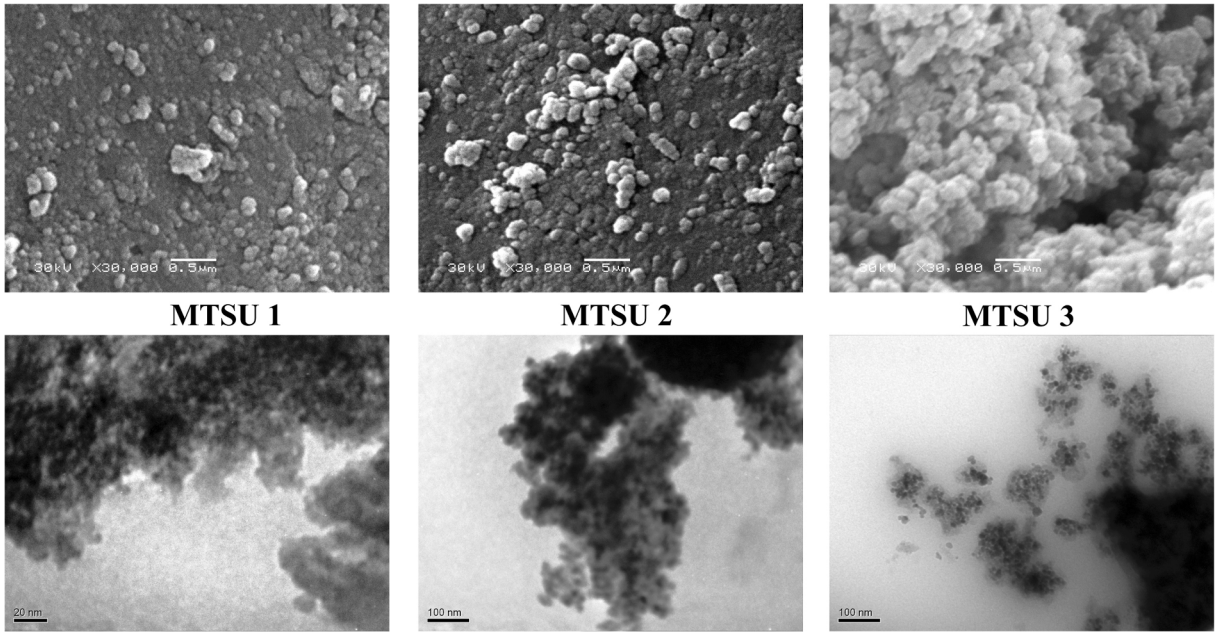

Fig. 3. SEM (*top*) and TEM (*bottom*) images of the magnetosensitive silica composites with thiourea groups.

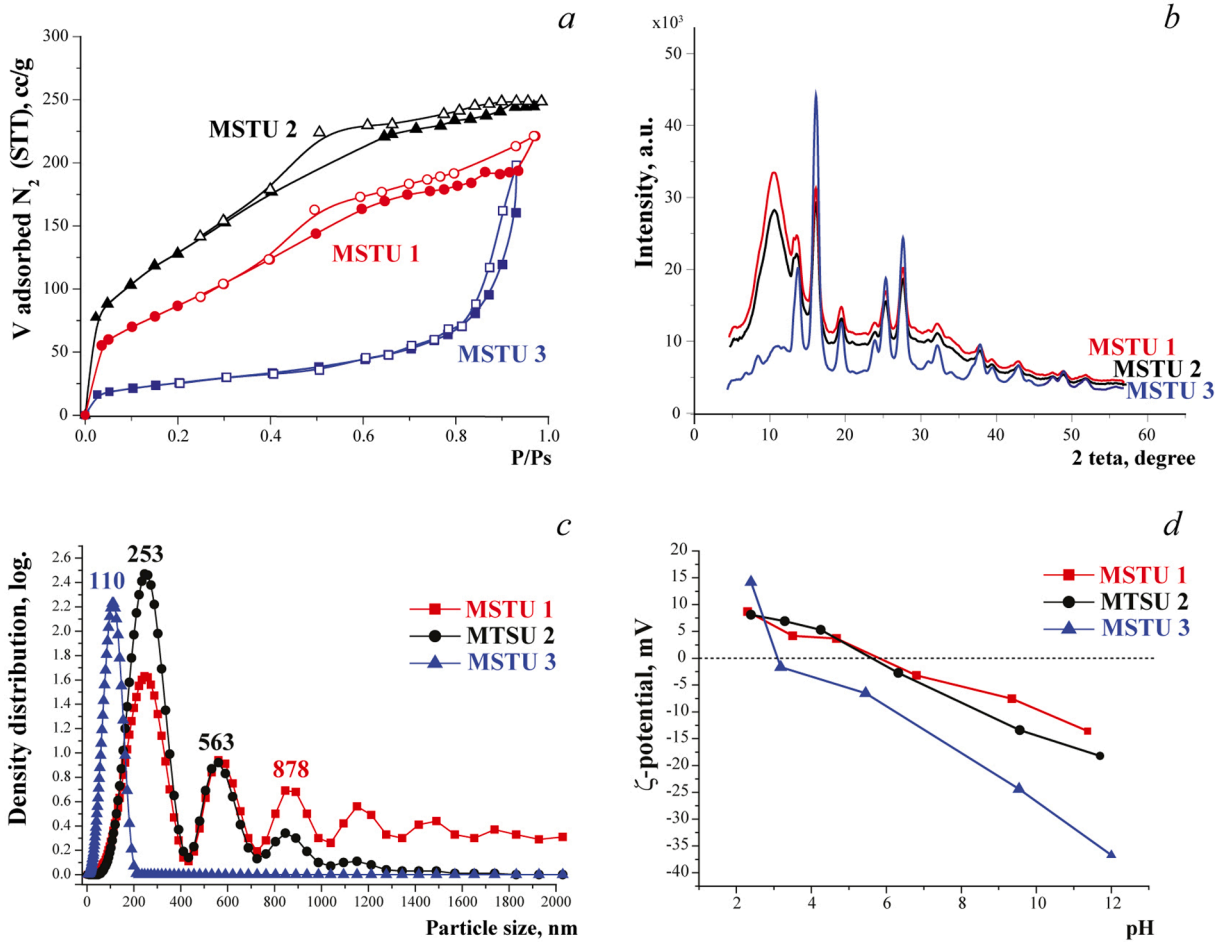

Fig. 4. Nitrogen adsorption–desorption isotherms (*a*), XRD powder patterns (*b*), PCCS data (*c*), and pH dependences of the ζ-potentials of dilute aqueous suspensions (*d*) for the obtained samples.

an error; therefore, the average values from these analyzes were used in all subsequent calculations. In the case of the **MSTU 3** sample, it was difficult to calculate the groups' content from TGA because other processes took place with the sample along with the extinction of functional groups (Fig. 2). Therefore, the loss of weight after 200 °C could not be uniquely correlated with the content of thiourea groups. Thus, the following concentration of thiourea groups was assumed for the samples **MSTU 1**–1.05, **MSTU 2**–0.68, **MSTU 3**–0.67 mmol/g.

According to the SEM microphotographs, the **MSTU 3** sample was characterized by loose particle arrangement (Fig. 3). Its particles were roughly-packed, and therefore this sample had the least value of specific surface (Fig. 4). The TEM image of the same sample showed that these particles had thin shells, which might be due to the low concentration of TEOS in the reaction mixture. Both **MSTU 1** and **MSTU 2** samples were composed not only of single magnetic particles but also of their agglomerates incorporated into silica shell. These particles were tightly packed, which resulted in higher specific surface. Thus, the features of the sol–gel process between TEOS and ETUS on the surface of magnetic particles were reflected in the SEM and TEM images in Fig. 3.

Fig. 4a shows isotherms of low-temperature nitrogen adsorption–desorption for the composite materials. The values of specific surface areas calculated using these isotherms are presented in Table 1. Isotherms measured for **MTSU 1** and **MTSU 2** samples could be attributed to type IV, having hysteresis loop of capillary condensation. Such type of isotherms is typical for xerogels and indicates the presence of mesopores in the structure of material. Sample **MTSU 3** had the lowest surface area and was similar to the original magnetite due to the slight change in the average particle size after functionalization. The nonlinear increase in the values of the specific surface area with linear increase in the TEOS content in the synthetic suspension was associated not so much with the size of the particles, but with their agglomeration and packaging.

The presence of magnetite was confirmed by the existence of appropriate reflections in the XRD patterns corresponding to the crystalline phase of magnetite (JCPDS card number 19–0629) (Fig. 4b). Moreover, the diffraction patterns witnessed about the thickness of the polysiloxane layer on the surface of magnetite particles. Thus, augmentation of polysiloxane shell for **MTSU 1** and **MTSU 2** samples was indicated by the presence of a broadened reflex at 11 deg. (2-theta), the appearance of which could be attributed to the presence of a certain amount of amorphous silica. The intensity of this reflexion was low when the content of the polysiloxane layer was minimal (sample **MTSU 3**). Also according to the calculation using Debye-Sherrer's equation, the size of the functionalized particles was calculated (see Table 1). These results showed difference, however, not significant, in particle size. Based on the fact that the size of the magnetite is 12.4 nm [32], in addition to the formation of polysiloxane shell, several magnetic particles apparently did stick together, confirming the TEM observations.

The actual size of the particles or their agglomerates in suspension was shown by PCC spectroscopic data (Fig. 4c). They indicated that in an aqueous suspension the agglomerates for the sample **MSTU 1** have dimensions of 253, 563 and 878 nm, with similar sizes of agglomerates for the sample **MSTU 2**, however, in smaller proportion. Sample **MSTU 3** was homogeneous in size with 110 nm in diameter. These data agreed with the data from other methods.

The electrokinetic potential arising at the phase boundary between a

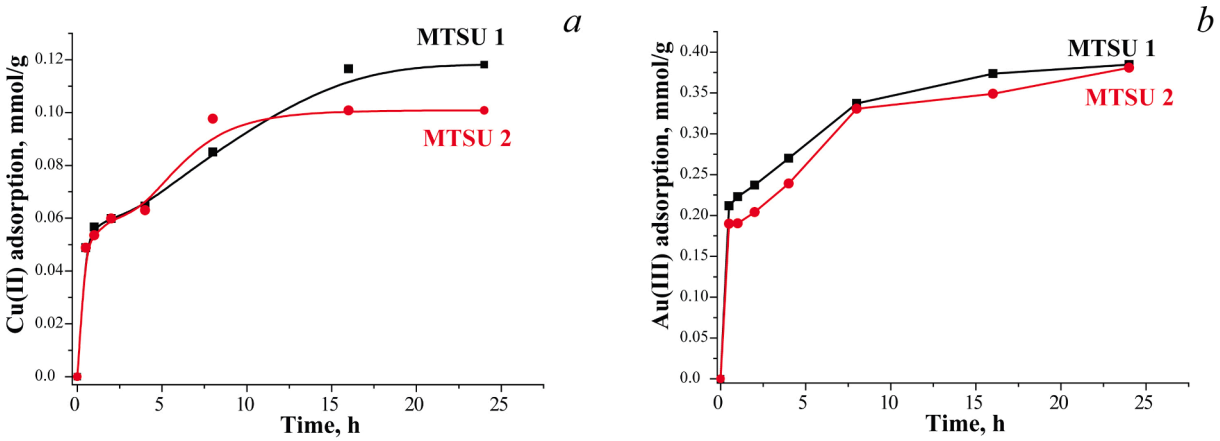

Fig. 5. The Cu(II) (*a*) and Au(III) (*b*) ions adsorption kinetic curves for thiourea-bearing synthesized materials (experimental data).

Table 2
Kinetic parameters of Cu(II) and Au(III) ions adsorption by the synthesized samples.

Sample (Metal ion)	Pseudo-first-order			Pseudo-second-order			
	A_{eq}, mmol/g	k_1,1/ min	R^2	A_{eq}, mmol/g	k_2,1/ mmol min	h, mmol/min g	R^2
MTSU 1 (Cu(II))	0.102	0.0039	0.885	0.128	0.0681	0.0009	**0.977**
MTSU 2 (Cu(II))	0.081	0.0061	0.836	0.107	0.1362	0.0014	**0.992**
MTSU 1 (Au(III))	0.205	0.0030	0.993	0.399	0.0387	0.0058	**0.996**
MTSU 2 (Au(III))	0.207	0.0021	0.912	0.397	0.0299	0.0043	**0.992**

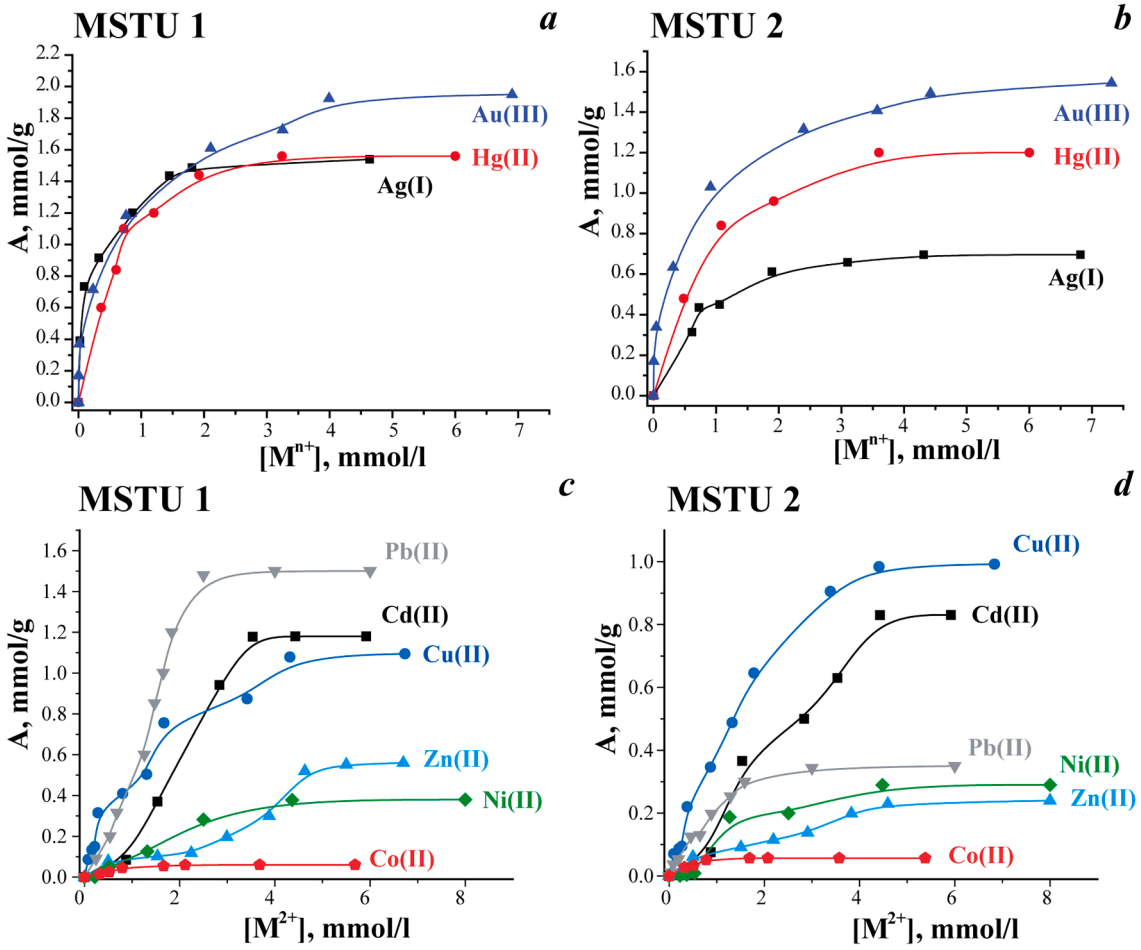

Fig. 6. Isotherms of metal ions adsorption at pH = 2 for **MSTU 1** *(a)* and **MSTU 2** *(b)* samples, as well at pH ~ 5 for **MSTU 1** *(c)* and **MSTU 2** *(d)* samples.

Table 3
Parameters of metal ions adsorption obtained by Langmuir and Freundlich isotherm equations.

Sample	M/Lig ratio	A_{exp}, mmol/g (mg/g)	K_d, mL/g	Langmuir equation			Freundlich equation	
				A_{max}, mmol/g	K_L, L/mmol	R^2	K_F, mmol/g	R^2
Ag(I)								
MSTU 1	1.5/1	1.54 (166.2)	7809	1.59	6.337	0.997	1.213	0.946
MSTU 2	1.0/1	0.70 (75.5)	465	0.78	1.487	0.994	0.439	0.824
			Hg(II)					
MSTU 1	1.5/1	1.56 (312.9)	1398	1.73	1.936	0.994	1.031	0.799
MSTU 2	1.8/1	1.20 (240.7)	653	1.38	1.292	0.994	0.713	0.862
Au(III)								
MSTU 1	1.9/1	1.95 (384.2)	41222	1.99	3.401	0.991	1.229	0.992
MSTU 2	2.3/1	1.55 (305.4)	35812	1.58	3.162	0.994	0.963	0.978
Cu(II)								
MSTU 1	1.0/1	1.09 (69.3)	941	1.34	0.679	0.966	0.443	0.951
MSTU 2	1.5/1	0.99 (62.9)	527	1.46	0.380	0.911	0.344	0.949
			Pb(II)					
MSTU 1	1.4/1	1.50 (310.8)	422	1.37	0.254	0.895	0.478	0.952
MSTU 2	0.5/1	0.35 (72.52)	316	0.43	0.880	0.969	0.195	0.962
Cd(II)								
MSTU 1	1.1/1	1.18 (132.7)	251	1.64	0.122	0.771	0.136	0.924
MSTU 2	1.2/1	0.83 (93.3)	170	1.31	0.242	0.715	0.271	0.925
Zn(II)								
MSTU 1	0.5/1	0.56 (36.6)	86	0.34	0.120	0.837	0.049	0.928
MSTU 2	0.4/1	0.24 (15.7)	71	0.36	0.278	0.842	0.083	0.926
Ni(II)								
MSTU 1	0.4/1	0.38 (22.3)	65	0.68	0.194	0.728	0.080	0.966
MSTU 2	0.4/1	0.29 (17.0)	45	0.48	0.246	0.683	0.042	0.920
Co(II)								
MSTU 1	0.06/1	0.06 (3.5)	47	0.07	1.486	0.976	0.036	0.750
MSTU 2	0.09/1	0.06 (3.5)	63	0.06	3.989	0.994	0.043	0.693

solid and a liquid under the action of a direct electric field is widely used to characterize the electrical properties of the surface. Changes in its values depending on the pH indicate the nature of the groups on the surface. Thus, the values of isoelectric points are shown in Table 1. For samples **MTSU 1** and **MTSU 2**, the points of zero charge were observed at pH values 5.8 and 5.5, respectively, while in the case of the sample **MTSU 3** there was a shift of pH to a more acidic region. This revealed the appearance on the surface of acidic groups not associated with –OH groups of magnetite, due to its isoelectric point at pH ~ 7 [37,38]. Such a shift could only be caused by the appearance of silanol groups (although IR spectroscopy did not detect them), because a large amount of ETUS silane with a bulk functional group was present in the reaction mixture, which affected the rate of hydrolysis and condensation [39,40].

3.2. Study of adsorption properties of materials to individual metal ions

The adsorption kinetics in this research was studied for two metal ions, namely Cu(II) and Au(III), for two samples **MTSU 1** and **MTSU 2** (Fig. 5). First, these studies indicated that the equilibrium was established after 16 h for both samples and metals, but about 90% of the metal ions were adsorbed already in 8 h. Second, the pseudo-second-order kinetic model gave a better fitting (Table 2) of the kinetic data and their R^2 was close to 1.0. This indicated the chemisorption mechanism for the interaction of the adsorbent with the adsorbate.

Fig. 6a,b shows the experimental isotherms of Ag(I), Au(III), and Hg (II) adsorption on the magnetite/silica/thiourea samples (for **MTSU 3** in Fig. SM4). The interpretation of experimental results was carried out using the Langmuir and Freundlich equations (Table 3). Ag(I), Au(III) and Hg(II) ions were chosen because of their affinity for sulfur, and they were very well adsorbed by the materials containing sulfur in an acidic environment. The results illustrated that the adsorption capacity decreased with decreasing thiourea groups concentration. However, the M/Lig ratios (Table 3) were higher than 1/1 in most cases. The ion-exchange mechanism of interaction is possible for silver(I) ions during the transformation of thiourea groups to mercapto groups with the formation of 1/1 complex: $\equiv Si(CH_2)_3\text{-}NH\text{-}C(=S)\text{–}NH\text{-}C_2H_5 \leftrightarrow \equiv Si(CH_2)_3\text{-}N{=}C(\text{-}SH)\text{–}NH\text{-}C_2H_5 + Ag^+ \rightarrow \equiv Si(CH_2)_3\text{-}N{=}C(\text{-}S\text{-}Ag)\text{–}NH\text{-}C_2H_5$. The same mechanism of adsorption could be realized for mercury (II) ions [33,38]. At first, mercury(II) ions can form metal/ligand complexes of 1/2, 1/1, and even 2/1, but the complexation tended to simplify with increasing metal concentration. There also could be observed the formation of polynuclear complexes: $[\equiv Si(CH_2)_3\text{-}N{=}C(\text{-}S\text{-})\text{–}NH\text{-}C_2H_5]_2Hg$, $\equiv Si(CH_2)_3\text{-}N{=}C(\text{-}S\text{-}Hg^+)\text{–}NH\text{-}C_2H_5$, $\equiv Si(CH_2)_3\text{-}N{=}C(\text{-}S\text{-}Hg\text{-}Hg^+)\text{–}NH\text{-}C_2H_5$ [41]. In the case of adsorption of gold(III) ions, which were present in the solution in the form of anions $[AuCl_4]^-$, there was a tendency for their interaction with the nitrogen of the thiourea group [42], which resulted in changes in the metal/ligand ratio. Therefore, explaining the metal/ligand ratio was sometimes not easy. The isotherms of Ag(I), Hg(II), and Au(III) ions adsorption by **MTSU 1** sample approached the y-axis in the region of low concentrations. Such type of isotherm indicated high affinity of the adsorbate to the adsorbent, which was reflected in the value of the distribution coefficient (K_d). All sorption isotherms (Fig. 6a,b) could be classified as classical L-isotherms (in due form) and were well described by the Langmuir equation, which indicated the formation of a monolayer.

The sorption capacity of the samples was determined as the maximum adsorption, A_{max}, which corresponded to the complete filling of the surface with a layer of the adsorbate. The data in Table 3 show that the isotherms for these three metal ions were well described by the Langmuir equation with high correlation coefficients. This indicated chemisorption on the surface of such materials. However, in case of adsorption of the gold(III) ions, the Freundlich model also had high correlation coefficients, indicating different energy centers on the surface with which the interaction took place, and could indirectly confirm that, in addition to the interaction with S, there was complexation with N of the thiourea group.

The values of the correlation coefficient R^2 were evaluated and compared in order to determine the best-fitting model for each sample and metal ion. So, according to the isotherms of copper(II) adsorption and parameters from Table 3, the experimental data were described reliably by both Langmuir and Freundlich models. This was evidenced by the correlation coefficients. At the same time, the distribution coefficients were rather high. In case of the **MSTU 2** sample, the distribution coefficients of some ions were even higher than for silver(I).

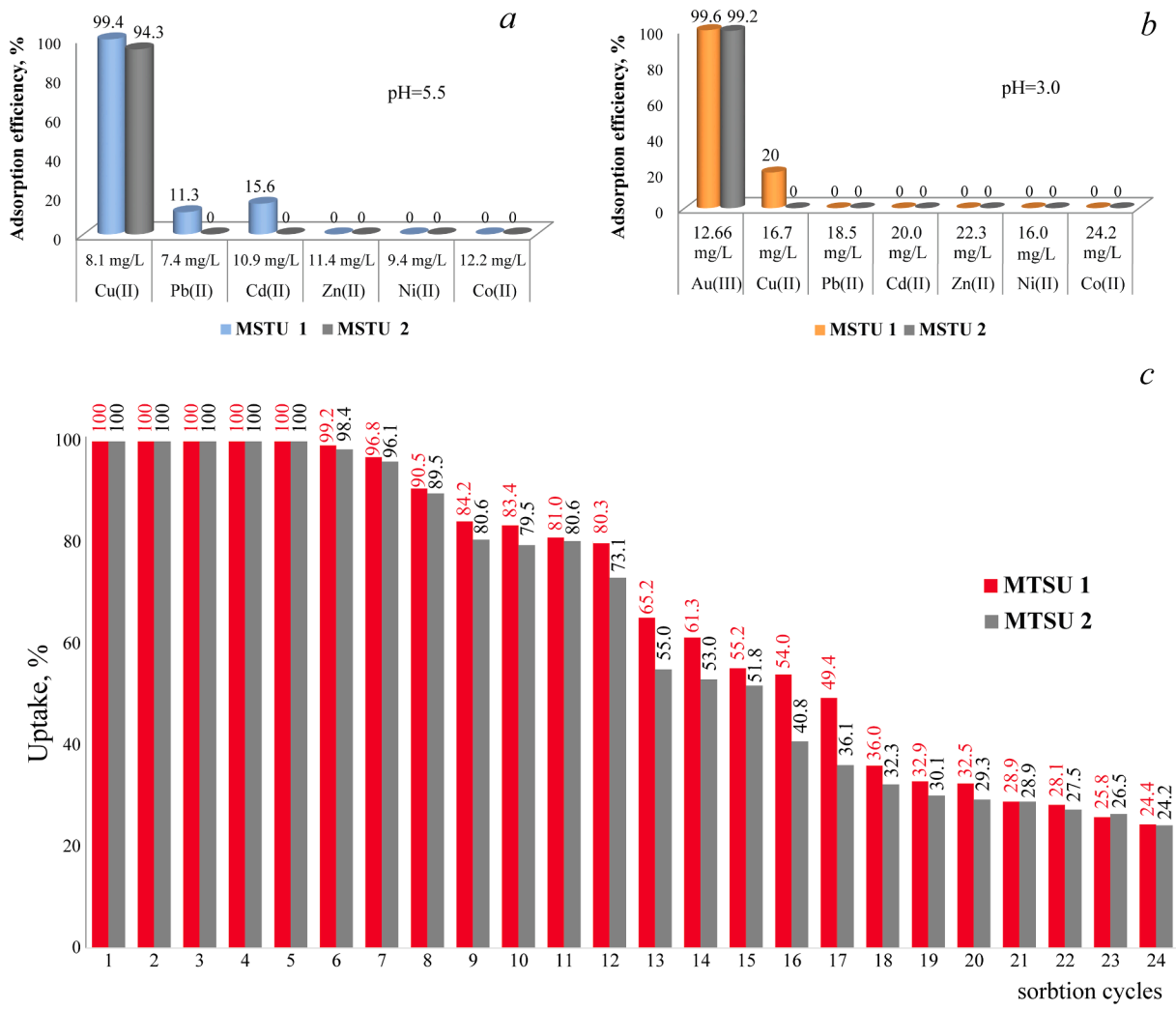

Fig. 7. Competitive adsorption of metal ions on adsorbents with thiourea groups at pH = 5.5 (*a*) and pH = 3 (*b*) in dynamic mode, and (*c*) concentrating of gold(III) ions from an ion mixture at pH = 3 on sorbent **MSTU 2** in 24 cycles without regeneration ($C[AuCl_4]^-$=12.66 mg/L).

Regarding the **MSTU 1** sample, isotherms of Pb(II), Cd(II), Zn(II), and Ni (II) adsorption together with fitting the results to Langmuir and Freundlich models showed that the adsorption process was not homogeneous, and it proceeded on heterogeneous surface.

The analysis of the findings proves that the process of adsorption of divalent ions by the magnetic materials with thiourea groups is ambiguous. The values of the distribution coefficients K_d calculated at low concentrations can be written in such order: Cu^{2+} (73 pm) > Pb^{2+} (119 pm) > Cd^{2+} (95 pm) > Zn^{2+} (74 pm) > Ni^{2+} (69 pm) > Co^{2+} (74.5 pm) [43]; however, the sorption capacities A_{exp} for ions of different sizes vary from sample to sample. But there is a general pattern: a higher number of functional groups causes a greater sorption capacity of the sample.

3.3. Research of competitive adsorption of metal ions on samples with thiourea groups. Desorption. Concentrating of gold ions in natural conditions

The next step was to study the adsorption on the obtained samples of other divalent metals from their water solutions (pH = 5.5). The fact is that contaminated industrial water contains a mixture of different metals, such as copper(II), cadmium(II), zinc(II), nickel(II), lead(II), and cobalt(II). Therefore, the sorption behavior of each metal ion separately and from their mixture was studied (Fig. 6c,d).

The study of metal ions adsorption from their mixture (Fig. 7a) of similar concentrations by sample **MSTU 1** shows that the sample preferably uptakes copper(II) ions, while some free adsorption centers are apparently occupied by lead(II) and cadmium(II). Sample **MSTU 2** probably has such content and location of functional groups that it contributes to the selective adsorption of copper(II) ions. When we reduced the concentrations of all ions ten times, except for copper(II), the same tendency persisted. When the concentration of copper(II) ions was also ten times reduced, it opened the possibility for all adsorption centers to uptake four metals (Fig. SM5). In addition to the features of the structure of the sorbents, such selectivity of sorption for copper(II) cations can be explained by the greater stability of copper(II) complexes in the Irving-Williams series: Mn^{2+}< Fe^{2+}< Co^{2+}<Ni^{2+}< Cu^{2+}>Zn^{2+} [44].

In the case of adsorption from a mixture at pH = 3 (Fig. 7b), the selective adsorption was caused by such factors as pH and high affinity of these groups to gold(III) ions. However, the sample **MTSU 1**, which had a large number of functional groups, also adsorbed copper(II) ions from the mixture. This meant that selectivity in relation to copper(II) and gold(III) ions could be achieved for a sample with a smaller number of groups, but, as shown above, the sample **MSTU 2** had a high distribution coefficient relative to Cu(II) and Au(III) and the largest sorption capacity (Fig. 6b, e, Table 3). Such selective adsorption enabled to concentrate the microquantities of gold(III) ions from the mixture in 24 cycles without adsorbent recovery (Fig. 7c). Up to 80% of the absorption still occurred in the 12th cycle. Concerning the regeneration of **MSTU 2**

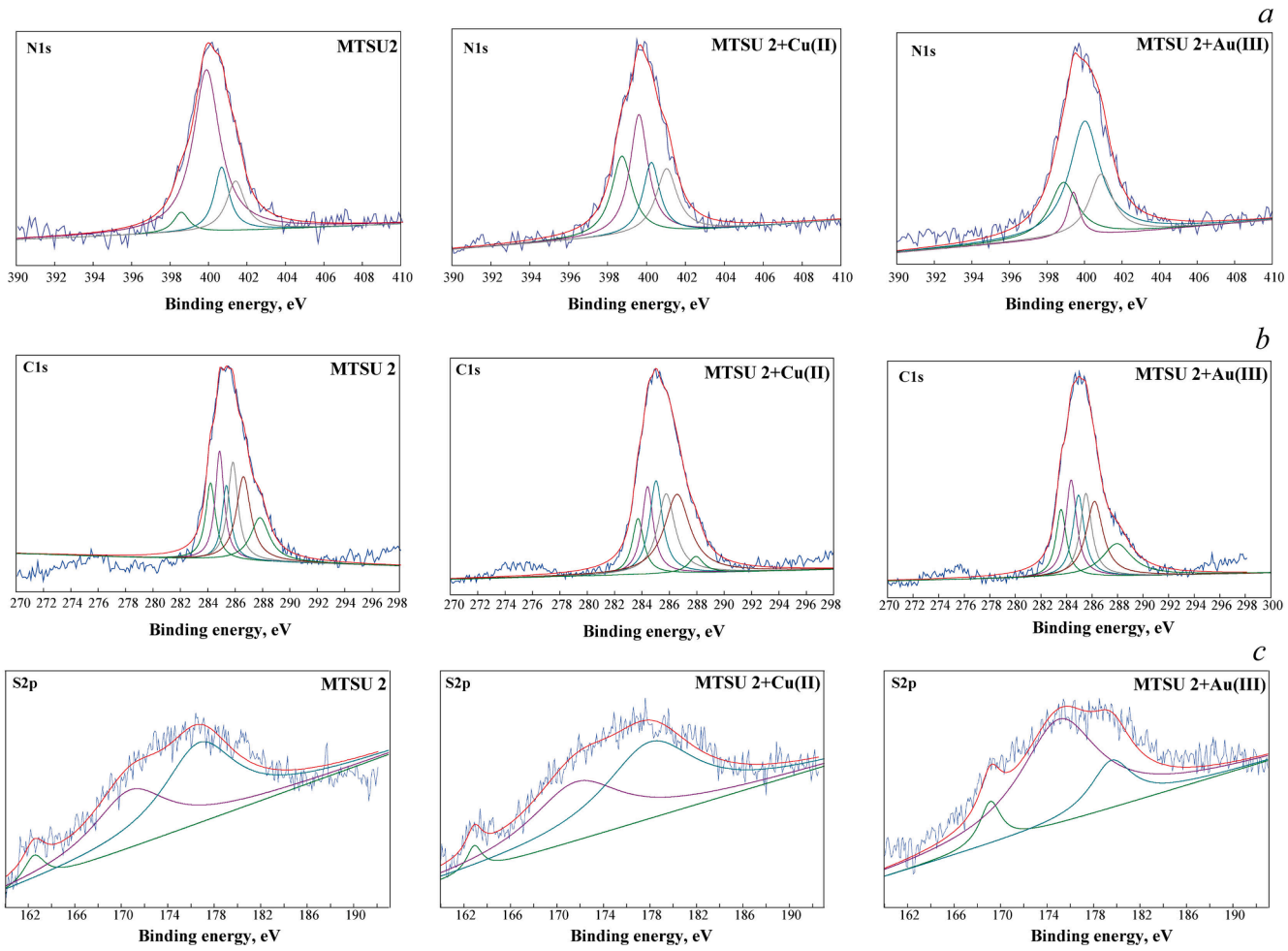

Fig. 8. X-ray photoelectron spectra of the (*a*) N1s, (*b*) C1s, (*c*) S2p for **MTSU 2** samples.

adsorbent, it was shown that 100% of adsorption–desorption of mercury (II) ions in 2 cycles was achieved using EDTA in an acidified solution, ~100% of gold(III) ions in an acidified water-alcohol solution of thiourea, and 98% for copper(II) in application of the last desorbing mixture.

Natural water was selected for the study, from a river flowing near the ore mountains, where there used to be copper mines. The river water was concentrated 25 times and this concentrate contained trace amounts of copper and gold (Table SM1). Adsorption of copper and gold ions from such water for samples with thiourea groups was at a high level, up to 61.8% for copper and up to 96.5% for gold. But at the same time, as for samples with thiol groups [45], the adsorption of other elements, such as Fe, Mn, Pb, Cd occurred also with high efficiency. The data of such non-selective adsorption from a mixture of ions, which are present in very small quantities in natural water, correlated with our experimental data when conducting adsorption from model solution (Fig. SM5). 9.6 μg of Cu(II) and 13 μg of Au(III) were leached from 1 g of the **MSTU 1** sample after passing river water through it for 6 days. Therefore, such samples are suitable for the concentration of gold and copper ions from natural water bodies.

3.4. Changes in the surface layer of the adsorbent with thiourea groups during the adsorption of copper (II) and gold(III) ions investigated by the XPS

XPS analysis was applied to observe the chemical state of each element and its environment in the pure **MTSU 2** sample and the same sample after sorption of copper(II) and gold(III) ions (Fig. 8, Table 4, Fig. SM6, SM7).

In order to establish the oxidation state of iron, XPS Fe3p and Fe2p spectra were recorded and analysed (Fig. SM6a,b). The Fe3p peaks were deconvoluted into the Fe^{2+}(54.75 eV) and Fe^{3+} (56.41 eV) [46] and their areas had an approximate ratio of 1:2 (Table 4), similar to the initial mixture of cations in magnetite. Fig. SM6b presents the peak positions of Fe2p3/2 and Fe2p1/2 at 710.76 and 724.19 eV, respectively. The main difference between magnetite and iron(III) oxide is the absence of a broadened satellite peak [46]. It should also be noted that the positions of the peaks did not undergo changes, which indicated that magnetite did not change during sorption in different pH ranges.

XPS Si2p spectra (Fig. SM6c, Table 4) demonstrated three peaks from 102.4 eV to 104.4 eV indicating the presence of three types of bonds with the silicon atom, namely Si-C, Si-O-Si, Si-O-Fe [47,48]. Deconvolution of the XPS O1s spectra (Table 4, Fig. SM6d) indicated the existence of non-hydrolyzed ethoxy groups, silanol groups (which is consistent with the IR spectra), as well as iron and silicon oxides. So, XPS Fe3p, Fe2p, Si2p and O1s spectra revealed the presence of Fe_3O_4, SiO_2 and organic groups, which was also confirmed by other methods (IR, elemental analysis, SEM-EDS).

It is known that the thiourea group exists in two tautomeric forms, thione –NH–C(=S) –NH– and thiol –N=C(–SH) –NH–, and in our previous work [49], the transformation of thione to the thiol form during the adsorption of silver(I) and mercury(II) ions in an acidic medium was shown by IR spectroscopy. The analysis of XPS N1s spectra (Fig. 8a) showed that the original **MSTU 2** sample had 4 peaks, which indicated the existence of both thione and thiol forms and a protonated –NH– group. During copper(II) adsorption, the area for the N—C peak did not increase significantly, which might indicate the absence of changes in

Table 4
XPS data and assignments for the **MTSU 2** samples.

MTSU 2	MTSU 2 + Cu(II)	MTSU 2 + Au(III)	*assignment*
Fe3p, BE, eV (% Area)			
54.75 (31.88)	54.79 (26.94)	54.55 (27.28)	*Fe(II)*
56.41 (68.12)	56.91 (73.06)	56.30 (72.72)	*Fe(III)*
Fe2p, BE, eV (% Area)			
710.76 (59.62)	710.73 (57.7)	710.67 (56.07)	*Fe 2p3/2*
724.19 (40.38)	724.12 (42.3)	724.25 (43.93)	*Fe 2p1/2*
Si2p, BE, eV (% Area)			
102.88 (34.32)	102.46 (38.34)	102.4 (29.12)	*Si-C*
103.68 (43.68)	103.34 (46.91)	103.18 (39.80)	*Si-O-Si*
104.43 (22.0)	104.19 (14.75)	104.1 (31.09)	*Si-O-Fe*
O1s, BE, eV (% Area)			
531.51 (17.08)	531.32 (25.92)	530.78 (9.54)	*O—C*
532.39 (34.76)	532.04 (28.14)	531.83 (31.29)	*O—H*
533.14 (34.15)	532.66 (29.23)	532.53 (32.7)	*O-Si*
533.89 (14.01)	533.4 (16.7)	533.28 (26.47)	*O-Fe*
N1s, BE, eV (% Area)			
398.59 (4.93)	398.74 (26.03)	398.89 (21.78)	*N—C*
399.90 (66.44)	399.62 (33.79)	399.45 (7.55)	*N—H*
400.69 (14.57)	400.25 (19.02)	400.03 (50.31)	*N═C*
401.41 (14.05)	401.04 (21.17)	401.01 (20.35)	NH_2^+
C1s, BE, eV (% Area)			
284.21 (14.01)	283.72 (9.87)	283.58 (12.00)	*C-Si*
284.87 (17.80)	284.42 (15.21)	284.37 (18.01)	*C—C, C—H*
285.37(12.22)	285.03 (18.60)	284.95 (15.73)	*C—S*
285.84 (18.37)	285.78 (21.48)	285.53 (16.24)	*C═N*
286.61 (22.40)	286.57 (31.07)	286.20 (21.58)	*C═S*
287.82 (15.21)	287.95 (3.77)	288.05 (16.43)	*C—N*
S2p, BE, eV (% Area)			
162.51 (5.54)	162.89 (3.15)	169.13 (8.30)	*S═C*
170.76 (40.45)	171.65 (41.95)	175.04 (73.71)	*S—C*
176.76 (54.02)	178.04 (54.9)	179.54 (17.99)	*S—C—N*
Cu2p, BE, eV (% Area)			
–	932.52 (39.65)	–	*Cu(II)*
–	941.36 (9.19)	–	*satellite*
–	952.20 (35.73)	–	*Cu(II)*
–	962.50 (15.43)	–	*satellite*
Au4f, BE, eV (% Area)			
–	–	84.07 (57.6)	*Au(III)*
–	–	87.62 (42.4)	*Au(III)*

the thione-thiol transformation, but the peak at 401.04 eV increased, which indicated interaction with the –NH– groups [50]. During the adsorption of gold(III) ions, the largest peak area was for the peaks related to the formation of the thiol form at 400.3 eV and $–NH_2^+–$ groups at 400.01 eV. These data confirmed our assumptions about the complex formation of metal ions with the –NH– groups as well (the sorption capacity of the metal in mmol/g exceeded the mmol/g of sulfur).

In the XPS spectra (Fig. 8b) of the initial sample, C1s was deconvoluted into six different carbon states at 284.21 eV, 284.87 eV, 285.37 eV, 285.84 eV, 286.61 eV, and 287.82 eV, which were attributed to CSi [51], C—C + C—H, C—S, C═N, C═S, C—N [52], respectively. Thus, all samples contained the thione and thiol forms of the thiocarbamate group (Table 4). The shifts were observed, however, in relation to the original sample, which indicated the interaction of these groups with metal ions.

The results of the XPS S1s spectra on the surface of magnetically controlled samples before and after adsorption of Cu(II) and Au(III) showed (Fig. 8c) that for the initial **MSTU 2** sample with thiourea groups there were three lines with binding energies at 162.51 eV, 170.76 eV and 176.76 eV, corresponding to sulfur in C═S, C—S and NC-S groupings, respectively [50,53]. After the adsorption of copper (II) ions, there was a little line shift (sometimes up to 1.0 eV) (Table 4), which might indicate the formation of a complex on the surface of the thiocarbamate group and Cu(II). For the **MTSU 2** sample loaded with gold(III), there was a significant shift of the peaks from 162.51 eV to 169.13 eV, which corresponded to the Me—S—C bond with thiolate compound formation [54]. Therefore, it could be concluded that in a neutral environment, when interacting with copper(II) ions, the thiourea group formed complexes on the surface and existed in the thione form, while when gold ions were sorbed in an acidic environment – it converted into the thiol one.

XPS of Cu2p spectrum presented in Figure SM7a demonstrated two peaks at 932.52 eV and 952.20 eV attributed to Cu2p3/2 and Cu2p1/2, respectively [42]. These peaks could be ascribed to the Cu(II) state. Two satellite peaks at 941.36 eV and 962.50 eV have been noted, which matched to the paramagnetic chemical state of Cu(II).

Figure SM7b shows the XPS of Au4f spectra of **MTSU 2** + Au(III). Biding energy at 84.07 and 87.62 eV could be assigned to free Au(III) [55] which indicated the Au(III) did not recover under such conditions.

4. Conclusions

Current research examined an approach to the synthesis of magnetite (Fe_3O_4) nanoparticles with polysiloxane shell containing thiourea groups using two-component system of TEOS and trifunctional silane $(C_2H_5O)_3Si(CH_2)_3$-NH-C(S)–NH-C_2H_5. The influence of such factors as the ratio and concentration of the reacting components and the nature of the catalyst on the porosity, the content and availability of functional groups, and the thickness of the silica layer were investigated. It was shown that the synthesized materials could be used for extraction of Hg^{2+}, Ag^+, Cu^{2+}, $[AuCl_4]^-$, Cd^{2+}, Pb^{2+}, and Zn^{2+} from aqueous solutions. It was determined that the sample with thiourea groups (0.68 mmol/g of functional groups and S_{sp} = 486 m^2/g) selectively adsorbed 94.3% of copper(II) and 99.2% of gold (III) ions from prepared aqueous solutions. As well it accumulated $[AuCl_4]^-$ ions on the surface of the sorbent up to 80% in 12 cycles without regeneration from the metal ions mixture containing 12.66 μg/L of Au(III). It was shown that such a magnetic sample could concentrate 9.6 μg/g of copper ions and 13 μg/g of gold ions from natural water and removed 61.8% of copper ions and 96.5% gold ions (pH = 6.8). XPS data confirmed the transition of the thiourea group's thione tautomeric form into a thiol in the acidic pH range and the existence of an unchanged thione at a pH close to neutral. It was found that the high sorption capacity of such sample for Cu(II) and Au(III) ions was also associated with the formation of complexes not only with sulfur in the thiourea groups, but with the nitrogen groups as well.

The approaches to the synthesis of hybrid organic–inorganic adsorption materials with controlled functionality of their surfaces stated above open new prospects for the sorption technology.

Declaration of Competing Interest

The authors declare that they have no known competing financial interests or personal relationships that could have appeared to influence the work reported in this paper.

Data availability

Data will be made available on request.

Acknowledgements

This work was supported by APVV-19-0302 project (Slovakia) and Swedish Research Council grant DNr.2018-04841 (Sweden).

Appendix A. Supplementary data

Supplementary data to this article can be found online at https://doi.org/10.1016/j.apsusc.2022.155253.

References

[1] N.Th.K. Thanh, Magnetic nanoparticles: from fabrication to clinical applications/ N.Th.K.Thanh - CRC Press, Taylor & Francis Group, Boca Raton, FL 2012. - 616 p. https://doi.org/10.1201/b11760.

[2] S.G. Krishnan, F.-L. Pua, F. Zhang, A review of magnetic solid catalyst development for sustainable biodiesel production, Biomass Bioenergy 149 (2021), 106099, https://doi.org/10.1016/j.biombioe.2021.106099.

[3] J. Cypriano, M. Bahri, K. Dembelé, W. Baaziz, P. Leão, D.A. Bazylinski, F. Abreu, O. Ersen, M. Farina, J. Werckmann, Insight on thermal stability of magnetite magnetosomes: implications for the fossil record and biotechnology, Sci. Rep. 10 (2020) 6706, https://doi.org/10.1038/s41598-020-63531-5.

[4] D. Mehta, S. Mazumdar, S.K. Singh, Magnetic adsorbents for the treatment of water/wastewater - A review, J. Water Process Eng. 7 (2015) 244–265, https://doi.org/10.1016/j.jwpe.2015.07.001.

[5] B. Kalska-Szostko, U. Wykowska, K. Piekut, D. Satuła, Stability of Fe_3O_4 nanoparticles in various model solutions, Colloids Surf. A 450 (2014) 15–24, https://doi.org/10.1016/j.colsurfa.2014.03.002.

[6] C. Su, Environmental implications and applications of engineered nanoscale magnetite and its hybrid nanocomposites: A review of recent literature, J. Hazard. Mater. 322 (2017) 48–84, https://doi.org/10.1016/j.jhazmat.2016.06.060.

[7] R.P. Pogorilyi, I.V. Melnyk, Y.L. Zub, S. Carlson, G. Daniel, P. Svedlindh, G. A. Seisenbaeva, V.G. Kessler, New product from old reaction: uniform magnetite nanoparticles from iron-mediated synthesis of alkali iodides and their protection from leaching in acidic media, RSC Adv. 4 (43) (2014) 22606–22612, https://doi.org/10.1039/C4RA02217C.

[8] I.M. El-Nahhal, N.M. El-Ashgar, A review on polysiloxane-immobilized ligand systems: synthesis, characterization and applications, J. Organomet. Chem. 692 (2007) 2861–2886, https://doi.org/10.1016/j.jorganchem.2007.03.009.

[9] H. Zheng, D. Hua, L. Zhang, C. Ma, T. Rufford, Thiol functionalized mesoporous silicas for selective adsorption of precious metals, Miner. Eng. 35 (2012) 20–26, https://doi.org/10.1016/j.mineng.2012.04.006.

[10] F. Ke, J. Jiang, Y. Li, J. Liang, X. Wan, S. Ko, Highly selective removal of Hg^{2+} and Pb^{2+} by thiol-functionalized Fe_3O_4@metal-organic framework core-shell magnetic microspheres, Appl. Surf. Sci. 413 (2017) 266–274, https://doi.org/10.1016/j.apsusc.2017.03.303.

[11] M.F. Hamza, A.-A.-H. Abdel-Rahman, M.A. Hawata, R.E. Araby, E. Guibal, A. Fouda, Y. Wei, N.A. Hamad, Functionalization of magnetic chitosan microparticles – Comparison of trione and trithione grafting for enhanced silver sorption and application to metal recovery from waste X-ray photographic films, J. Environ. Chem. Eng. 10 (3) (2022), 107939, https://doi.org/10.1016/j.jece.2022.107939.

[12] H. Lin, L. Chen, J. Ou, Z. Liu, H. Wang, J. Dong, H. Zou, Preparation of well-controlled three-dimensional skeletal hybrid monoliths via thiol–epoxy click polymerization for highly efficient separation of small molecules in capillary liquid chromatography, J. Chromatogr. A 1416 (2015) 74–82, https://doi.org/10.1016/j.chroma.2015.09.011.

[13] R.P. Pogorilyi, I.V. Melnyk, Y.L. Zub, G.A. Seisenbaeva, V.G. Kessler, Immobilization of urease on magnetic nanoparticles coated by polysiloxane layers bearing thiol- or thiol- and alkyl-functions, J. Mater. Chem. B 2 (2014) 2694–2702, https://doi.org/10.1039/c4tb00018h.

[14] Q. Zhao, C. Wang, Y. Liu, J. Wang, Y. Gao, X. Zhang, T. Jiang, S. Wang, PEGylated mesoporous silica as a redox-responsive drug delivery system for loading thiol-containing drugs, Int. J. Pharm. 477 (2014) 613–622, https://doi.org/10.1016/j.ijpharm.2014.10.056.

[15] Y. Fang, Y. Chen, X. Li, X. Zhou, J. Li, W. Tang, J. Huang, J. Jin, J. Ma, Gold on thiol-functionalized magnetic mesoporous silica sphere catalyst for the aerobic oxidation of olefins, J. Mol. Catal. A: Chem. 392 (2014) 16–21, https://doi.org/10.1016/j.molcata.2014.04.032.

[16] V.V. Tomina, I.M. Furtat, N.V. Stolyarchuk, Y.L. Zub, M. Kanuchova, M. Vaclavikova, I.V. Melnyk, Chapter 2 - Surface and structure design of aminosilica nanoparticles for multifunctional applications: adsorption and antimicrobial studies, Editor(s): Inna V. Melnyk, Miroslava Vaclavikova, Gulaim A. Seisenbaeva, Vadim G. Kessler, In Micro and Nano Technologies, Biocompatible Hybrid Oxide Nanoparticles for Human Health, Elsevier, 2019, 15-31, ISBN 9780128158753. https://doi.org/10.1016/B978-0-12-815875-3.00002-3.

[17] S.H. Im, T. Herricks, Y.T. Lee, Y. Xia, Synthesis and characterization of monodisperse silica colloids loaded with superparamagnetic iron oxide nanoparticles, Chem. Phys. Lett. 401 (2005) 9–23, https://doi.org/10.1016/j.cplett.2004.11.028.

[18] H. Hu, Z. Wang, L. Pan, Synthesis of monodisperse Fe_3O_4@silica core–shell microspheres and their application for removal of heavy metal ions from water, J. Alloy. Compd. 492 (1–2) (2010) 656–661, https://doi.org/10.1016/j.jallcom.2009.11.204.

[19] S. Alam, C. Anand, R. Logudurai, V.V. Balasubramanian, K. Ariga, A.C. Bose, T. Mori, P. Srinivasu, A. Vinu, Comparative study on the magnetic properties of iron oxide nanoparticles loaded on mesoporous silica and carbon materials with different structure, Micropor. Mesopor. Mater. 121 (2009) 178–184, https://doi.org/10.1016/j.micromeso.2009.01.029.

[20] L. Li, E.S.G. Choo, J. Yi, J. Ding, X. Tang, J. Xue, Superparamagnetic silica composite nanospheres (SSCNs) with ultrahigh loading of iron oxide nanoparticles via an oil-in-DEG microemulsion route, Chem. Mater. 20 (2008) 6292–6294, https://doi.org/10.1021/cm8012107.

[21] D. Angelova, L. Armelao, S. Gross, G. Kickelbick, R. Seraglia, E. Tondello, G. Trimmel, A. Venzo, Investigation of thiourea-silanes as viable precursors for the sol–gel synthesis of composites containing Zn–S complexes, Appl. Surf. Sci. 226 (2004) 144–148, https://doi.org/10.1016/j.apsusc.2003.11.014.

[22] S.H. Lee, S.S. Park, S. Parambadath, C.-S. Ha, Sulphonic acid functionalized periodic mesoporous organosilica with the bridged bissilylated urea groups for high selective adsorption of cobalt ion from artificial seawater, Micropor. Mesopor. Mater. 226 (2016) 179–190, https://doi.org/10.1016/j.micromeso.2015.10.047.

[23] R. Ou, W. Zhu, L. Li, X. Wang, Q. Wang, Q. Gao, A. Yuan, J. Pan, F. Yang, Boosted capture of volatile organic compounds in adsorption capacity and selectivity by rationally exploiting defect-engineering of UiO-66(Zr), Sep. Purif. Technol. 266 (2021), 118087, https://doi.org/10.1016/j.seppur.2020.118087.

[24] W. Li, W. Tu, J. Cheng, F. Yang, X. Wang, L. Li, D. Shang, X. Zhou, C. Yu, A. Yuan, J. Pan, Tuning N-doping thermal-process enables biomass-carbon surface modification for potential separation effect of $CO_2/CH_4/N_2$, Sep. Purif. Technol. 282 (A) (2022), 120001, https://doi.org/10.1016/j.seppur.2021.120001.

[25] N. Karthik, M.G. Sethuraman, Surface protection of copper by allyl thiourea and hybrid sol–gel coatings, Prog. Org. Coat. 90 (2016) 380–389, https://doi.org/10.1016/j.porgcoat.2015.08.004.

[26] S. Peng, Z. Zeng, W. Zhao, H. Li, Q. Xue, X. Wu, Synergistic effect of thiourea in epoxy functionalized silica sol–gel coating for copper protection, Surf. Coat. Technol. 213 (2012) 175–182, https://doi.org/10.1016/j.surfcoat.2012.10.043.

[27] M. Mureseanu, A. Reiss, N. Cioatera, I. Trandafir, V. Hulea, Mesoporous silica functionalized with 1-furoyl thiourea urea for Hg(II) adsorption from aqueous media, J. Hazard. Mater. 182 (2010) 197–203, https://doi.org/10.1016/j.jhazmat.2010.06.015.

[28] T.-L. Lin, H.-L. Lien, Effective and selective recovery of precious metals by thiourea modified magnetic nanoparticles, Int. J. Mol. Sci. 14 (2013) 9834–9847, https://doi.org/10.3390/ijms14059834.

[29] G.I. Nazarchuk, I.V. Melnyk, Y.L. Zub, O.I. Makridina, A.I. Vezentsev, Mesoporous silica containing $\equiv Si(CH_2)_3NHC(S)NHC_2H_5$ functional groups in the surface layer, J. Colloid Interface Sci. 389 (2013) 115–120, https://doi.org/10.1016/j.jcis.2012.08.057.

[30] Z. Ma, Y. Guan, H. Liu, Superparamagnetic silica nanoparticles with immobilized metal affinity ligands for protein adsorption, J. Magn. Magn. Mater. 301 (2006) 469–477, https://doi.org/10.1016/j.jmmm.2005.07.027.

[31] Y. Zhu, Z.-S. Bai, H.-L. Wang, Microfluidic synthesis of thiourea modified chitosan microsphere of high specific surface area for heavy metal wastewater treatment, Chin. Chem. Lett. 28 (3) (2017) 633–641, https://doi.org/10.1016/j.cclet.2016.10.031.

[32] I.V. Mel'nik, Y.L. Zub, B. Alonso, N.V. Abramov, P.P. Gorbik, Creation of a functional polysiloxane layer on the surface of magnetic nanoparticles using the sol–gel method, Glass Phys. Chem 38 (1) (2012) 96–104.

[33] I.V. Mel'nik, N.V. Stolyarchuk, L.I. Kozhara, V.P. Goncharik, Y.L. Zub, Synthesis of bridged polysilsesquioxane xerogels with thiourea groups, Russ. J. Gen. Chem. 83 (8) (2013) 1613–1620, https://doi.org/10.1134/S1070363213080240.

[34] I.V. Melnyk, O.I. Gona, L.I. Kozhara, Yu.L. Zub, N.A. Yaroshenko, T.F. Kuznetsova, A.I. Ratko, Study of Hg(II) sorption from its water solution by mesoporous silica with thiourea functional groups, 2008, in book "Sol-Gel Methods for Materials Processing (ARW NATO)" / Eds. P.Innocenzi, Yu.L. Zub and V.G. Kessler, Springer: Dordrecht, 2008, 375–381 (ISBN-13: 978-1402085222). http://doi.org/10.1007/978-1-4020-8514-7_31.

[35] M.A. Zayed, N.G. Imam, M.A. Ahmed, D.H. El Sherbiny, Spectrophotometric analysis of hematite/magnetite nanocomposites in comparison with EDX and XRF techniques, J. Mol. Liq. 231 (2017) 288–295, https://doi.org/10.1016/j.molliq.2017.02.007.

[36] Y.H. Chen, Thermal properties of nanocrystalline goethite, magnetite, and maghemite, J. Alloy. Compd. 553 (2013) 194–198, https://doi.org/10.1016/j.jallcom.2012.11.102.

[37] F. Vereda, A. Martín-Molina, R. Hidalgo-Alvarez, M. Quesada-Pérez, Specific ion effects on the electrokinetic properties of iron oxide nanoparticles: experiments and simulations, PCCP 17 (2015) 17069–17078, https://doi.org/10.1039/C5CP01011J.

[38] N. Kusyak, A. Kusyak, A. Petranovska, I. Melnyk, P. Gorbyk, Hg(II) ions adsorption study on DMSA-functionalized nanoscale magnetite, Mater. Today:. Proc. 62 (15) (2022) 7738–7744, https://doi.org/10.1016/j.matpr.2022.04.367.

[39] C.J. Brinker, Hydrolysis and condensation of silicates: Effects on structure, J. Non-Cryst. Solids 100 (1–3) (1988) 31–50, https://doi.org/10.1016/0022-3093(88)90005-1.

[40] A.A. Issa, A.S. Luyt, Kinetics of alkoxysilanes and organoalkoxysilanes polymerization: a review, Polymers 11 (2019) 537, https://doi.org/10.3390/polym11030537.

[41] A.M.T. Bell, J.M. Charnock, G.R. Helz, A.R. Lennie, F.R. Livens, J.F. W. Mosselmans, R.A.D. Pattrick, D.J. Vaughan, Evidence for dissolved polymeric mercury(II)-sulfur complexes? Chem. Geol. 243 (2007) 122–127, https://doi.org/10.1016/j.chemgeo.2007.05.013.

[42] B. Zhang, S. Wang, L. Fu, L. Zhang, J. Zhao, C. Wang, Selective high capacity adsorption of Au(III) from aqueous solution by poly(glycidyl methacrylate) functionalized with 2,6-diaminopyridine, Polym. Bull. 76 (2019) 4017–4033, https://doi.org/10.1007/s00289-018-2594-5.

[43] S.I. Gorelsky, L. Basumallick, J. Vura-Weis, R. Sarangi, K.O. Hodgson, B. Hedman, K. Fujisawa, E.I. Solomon, Spectroscopic and DFT investigation of [M{HB(3,5-iPr2pz)3}(SC6F5)] (M = Mn, Fe Co, Ni, Cu, and Zn) model complexes: periodic trends in metal−thiolate bonding, Inorg. Chem. 44 (14) (2005) 4947–4960, https://doi.org/10.1021/ic050371m.

[44] I.V. Melnyk, R.P. Pogorilyi, Y.L. Zub, M. Vaclavikova, K. Gdula, A. Dąbrowski, G. A. Seisenbaeva, V.G. Kessler, Protection of thiol groups on the surface of magnetic

adsorbents and their application for wastewater treatment, Sci. Rep. 8 (2018) 8592, https://doi.org/10.1038/s41598-018-26767-w.
[45] T. Yamashita, P. Hayes, Analysis of XPS spectra of Fe^{2+} and Fe^{3+} ions in oxide materials, Appl. Surf. Sci. 254 (8) (2008) 2441–2449, https://doi.org/10.1016/j.apsusc.2007.09.063.
[46] U. Eduok, O. Faye, J. Szpunar, M. Khaled, Effect of silylating agents on the superhydrophobic and self-cleaning properties of siloxane/polydimethylsiloxane nanocomposite coatings on cellulosic fabric filters for oil–water separation, RSC Adv. 11 (2021) 9586–9599, https://doi.org/10.1039/D0RA10565A.
[47] L. Zhai, B. Zhang, H. Liang, H. Wu, X. Yang, G. Luo, S. Zhao, Y. Qin, The selective deposition of Fe species inside ZSM-5 for the oxidation of cyclohexane to cyclohexanone, Science China Chemistry 64 (2021) 1088–1095, https://doi.org/10.1007/s11426-020-9968-x.
[48] I.V. Melnyk, G.I. Nazarchuk, M. Václavíková, Y.L. Zub, IR spectroscopy study of SBA-15 silicas functionalized with the ethylthiocarbamidepropyl groups and their interactions with Ag(I) and Hg(II) ions, Appl. Nanosci. 9 (2019) 683–694, https://doi.org/10.1007/s13204-018-0761-5.
[49] X. Huang, X. Cao, W. Wang, H. Zhong, Z. Cao, Preparation of a novel resin with acyl and thiourea groups and its properties for Cu(II) removal from aqueous solution, J. Environ. Manage. 204 (2017) 264–271, https://doi.org/10.1016/j.jenvman.2017.09.007.
[50] W. Lu, A.T. Tarekegne, Y. Ou, S. Kamiyama, H. Ou, Temperature-dependent photoluminescence properties of porous fluorescent SiC, Sci. Rep. 9 (2019) 16333, https://doi.org/10.1038/s41598-019-52871-6.
[51] C. Varodi, F. Pogăcean, A. Cioriță, O. Pană, C. Leoștean, B. Cozar, T. Radu, M. Coroș, R.I. Ștefan-van Staden, S.-M. Pruneanu, Nitrogen and sulfur co-doped graphene as efficient electrode material for L-cysteine detection, Chemosensors 9 (2021) 146, https://doi.org/10.3390/chemosensors9060146.
[52] D. Chen, C. Gan, X. Fan, L. Zhang, W. Li, M. Zhu, X. Quan, Improving the dynamic mechanical properties of XNBR using ILs/KH550-functionalized multilayer graphene, Materials 12 (17) (2019) 2800, https://doi.org/10.3390/ma12172800.
[53] F. Benseba, Y. Zhou, Y. Deslandes, E. Kruus, T.H. Ellis, XPS study of metal–sulfur bonds in metal–alkanethiolate materials. Surf. Sci. 405 (1998) L472–L476, PII: S0039-6028(98)00097-1.
[54] S. Adhikari, D. Sarkar, G. Madras, Hierarchical design of CuS architectures for visible light photocatalysis of 4-chlorophenol, ACS Omega 2 (7) (2017) 4009–4021, https://doi.org/10.1021/acsomega.7b00669.